Ready. Set. 2.0!

The NEW SunCHECK™

INDEPENDENT QA.
YOUR WAY.

"Having patient information, having machine information all in one easily accessible place... ***that's basically what you would want in a system.***"

Robert Staton, Ph.D., UF Health Cancer Center at Orlando Health, Orlando, FL

Learn more at:
sunnuclear.com

Platform

Patient

Machine

SUN NUCLEAR corporation

The relative biological effectiveness for carbon, nitrogen, and oxygen ion beams using passive and scanning techniques evaluated with fully 3D silicon microdosimeters

Linh T. Tran,[a] David Bolst, Susanna Guatelli, Alex Pogossov, Marco Petasecca, and Michael L. F. Lerch
Centre for Medical Radiation Physics, University of Wollongong, Wollongong, NSW 2522, Australia

Lachlan Chartier, Dale A. Prokopovich, and Mark I. Reinhard
NSTLI Nuclear Stewardship Platform, Australian Nuclear Science and Technology Organisation, Lucas Heights, NSW 2234, Australia

Marco Povoli and Angela Kok
SINTEF, 0373 Oslo, Norway

Vladimir L. Perevertaylo
SPA-BIT, Kiev, Ukraine

Naruhiro Matsufuji
National Institutes for Quantum and Radiological Science and Technology, Chiba, Japan

Tatsuaki Kanai
Gunma Heavy Ion Medical Centre, Gunma, Japan

Michael Jackson
University of New South Wales, Sydney, NSW 2052, Australia

Anatoly B. Rosenfeld[a]
Centre for Medical Radiation Physics, University of Wollongong, Wollongong, NSW 2522, Australia

(Received 29 December 2017; revised 7 March 2018; accepted for publication 7 March 2018; published 10 April 2018)

Background: The aim of this study was to measure the microdosimetric distributions of a carbon pencil beam scanning (PBS) and passive scattering system as well as to evaluate the relative biological effectiveness (RBE) of different ions, namely ^{12}C, ^{14}N, and ^{16}O, using a silicon-on-insulator (SOI) microdosimeter with well-defined 3D-sensitive volumes (SV). Geant4 simulations were performed with the same experimental setup and results were compared to the experimental results for benchmarking.

Method: Two different silicon microdosimeters with rectangular parallelepiped and cylindrical shaped SVs, both 10 μm in thickness were used in this study. The microdosimeters were connected to low noise electronics which allowed for the detection of lineal energies as low as 0.15 keV/μm in tissue. The silicon microdosimeters provide extremely high spatial resolution and can be used for in-field and out-of-field measurements in both passive scattering and PBS deliveries. The response of the microdosimeters was studied in 290 MeV/u ^{12}C, 180 MeV/u ^{14}N, 400 MeV/u ^{16}O passive ion beams, and 290 MeV/u ^{12}C scanning carbon therapy beam at heavy ion medical accelerator in Chiba (HIMAC) and Gunma University Heavy Ion Medical Center (GHMC), Japan, respectively. The microdosimeters were placed at various depths in a water phantom along the central axis of the ion beam, and at the distal part of the Spread Out Bragg Peak (SOBP) in 0.5 mm increments. The RBE values of the pristine Bragg peak (BP) and SOBP were derived using the microdosimetric lineal energy spectra and the modified microdosimetric kinetic model (MKM), using MKM input parameters corresponding to human salivary gland (HSG) tumor cells. Geant4 simulations were performed in order to verify the calculated depth-dose distribution from the treatment planning system (TPS) and to compare the simulated dose-mean lineal energy to the experimental results.

Results: For a 180 MeV/u ^{14}N pristine BP, the dose-mean lineal energy $\overline{y_D}$ obtained with two types of silicon microdosimeters started from approximately 29 keV/μm at the entrance to 92 keV/μm at the BP, with a maximum value in the range of 412 to 438 keV/μm at the distal edge. For 400 MeV/u ^{16}O ions, the dose-mean lineal energy $\overline{y_D}$ started from about 24 keV/μm at the entrance to 106 keV/μm at the BP, with a maximum value of approximately 381 keV/μm at the distal edge. The maximum derived RBE_{10} values for ^{14}N and ^{16}O ions were found to be 3.10 ± 0.47 and 2.93 ± 0.45, respectively. Silicon microdosimetry measurements using pencilbeam scanning ^{12}C ions were also compared to the passive scattering beam.

Conclusions: These SOI microdosimeters with well-defined three-dimensional (3D) SVs have applicability in characterizing heavy ion radiation fields and measuring lineal energy deposition with sub-millimeter spatial resolution. It has been shown that the dose-mean lineal energy increased significantly at the distal part of the BP and SOBP due to very high LET particles. Good agreement was observed for the experimental and simulation results obtained with silicon microdosimeters in ^{14}N and ^{16}O ion beams, confirming the potential application of SOI microdosimeter with 3D SV for quality assurance in charged particle therapy. [https://doi.org/10.1002/mp.12874]

Key words: heavy ion therapy, microdosimetry, MKM, RBE, silicon on insulator

1. INTRODUCTION

Particle therapy is particularly advantageous for the treatment of solid tumors compared to conventional electron and photon therapy due to a highly localized energy deposition. Therapeutic ion beams offer a depth-dose distribution with a pronounced maximum Bragg peak (BP) and sharp dose fall-off at large penetration depths, in contrast to the exponential dose deposition of photons or the broad maximum produced by electrons. Heavier ions such as carbon, nitrogen and oxygen have further advantages over protons and lighter ions for treating deep-seated radio-resistant tumors due to an increased relative biological effectiveness (RBE) in the stopping region at the BP, while sparing the normal tissue surrounding the tumor.

The potential limitations of using different particles species for cancer treatment have been discussed by Tommasino.[1] Oxygen ions are considered particularly promising due to an enhanced RBE in the target and are especially useful for the treatment of hypoxic tumors. However, higher entrance dose remains a drawback when using heavier ions.[1] Moreover, heavier ions require more sophisticated treatment planning systems due to a strong rise in RBE that corresponds to an increased ionization density in the individual tracks of the heavy charged particles.[2] Furthermore, it was shown that the maximum RBE of ions does not necessarily coincide with the maximum physical dose of the BP but it is shifted to greater LET values for heavier ions with increasing atomic numbers.[2] Therefore, it is important to evaluate the maximum RBE value depending on the ion energy and atomic number and its relation to the BP position to accurately prescribe the biological dose to be delivered to the tumor.

Various types of detectors can be used to measure microdosimetric quantities and derive RBE in heavy ion charged particle fields using radiobiological models. A conventional microdosimeter uses a tissue equivalent proportional counter (TEPC) that incorporates a spherical SV filled with tissue-equivalent gas that model micron-sized biological cells using low-pressure gas. While the TEPC is the gold standard for microdosimetry its large physical size means that spatial resolution is limited, with the addition of pile-up effects in therapeutic ion beams. Additionally, the TEPC's high voltage bias and gas supply requirements make it less ideal for routine QA in clinical environments. For this reason, experimental microdosimetric parameters have never been obtained at the Bragg peak and its distal part with high spatial resolution using a conventional TEPC.

Recently, a miniature TEPC developed by the group at INFN Legnaro laboratories was proposed to avoid pile up and assess the RBE of the radiation by linking the physical microdosimetric parameters with the corresponding biological response.[3] Studies using the TEPC for microdosimetric measurements for both in-field and out-of-field in low dose rate ^{12}C and ^{7}Li ion pencil beams have also been reported.[4,5]

Solid-state microdosimeters have been under development for the last two decades. A silicon monolithic ΔE-E detector with a very thin 1.8 μm ΔE stage and 500 μm thick E stage as well as a pixelated ΔE stage were introduced at Politechnico di Milano, Italy. They have been described and applied for neutron microdosimetry[6] and in proton therapy for RBE evaluation in a distal part of the Bragg peak[7] utilizing ΔE stage for LET measurements and E stage for recoil proton energy measurements (up to 8 MeV) followed by tissue-equivalent correction of LET spectrum event by event.

Silicon-on-insulator (SOI) microdosimetry was introduced at the Centre for Medical Radiation Physics (CMRP), University of Wollongong, Australia and is based on an array of micron-sized sensitive volumes (SV) mimicking the dimensions of cells. These microdosimeters are used for determining the energy deposited event by event produced by primary and secondary charged particles. The SOI microdosimeter has the advantages of having a small SV size (of the order of 10 μm thickness), low operational bias (5–10 V), and a high spatial resolution of the order of 100 μm which is limited by the accuracy of placing the microdosimeter in a phantom. Progress in the development of SOI microdosimeters at the CMRP and monolithic silicon ΔE-E detectors for microdosimetry and their applications in proton, heavy ion and neutron fields were well outlined in Ref. [8] and references within.

In this paper, we present measurements taken with two SOI microdosimeters, consisting of an array of freestanding 3D sensitive volumes (SVs). The microdosimeters have the size of the order of cellular dimensions with a 10 μm thickness, known as the Bridge and Mushroom microdosimeters. The microdosimeters were used to measure the dose-mean

lineal energy deposition profiles for ^{12}C, ^{14}N, and ^{16}O ion fields with subhundred micron spatial resolution close to and at the distal part of the BP and SOBP. Such precise measurements cannot be achieved using the conventional TEPC due to its large physical size. The microdosimetric spectra obtained with the SOI microdosimeter at various depths in water for different ions are presented and compared to Geant4 simulation results. The newly developed mushroom microdosimeter could also operate in a high-dose rate scanning beam of 290 MeV/u ^{12}C ions without pile-up problems, with the dose-mean lineal energy deposition profiles in water being successfully obtained. Measured dose-mean lineal energy for different ion species and based on that the RBE_{10} values corresponding to 10% of human salivary gland (HSG) cell survival calculated based on the modified microdosimetric kinetic model are also presented.

2. MATERIALS AND METHODS

2.A. SOI microdosimeters and microplus probe

Two types of silicon-on-insulator (SOI) microdosimeters were used in this study. The first microdosimeter design is called the "bridge" microdosimeter, consisting of an array of 4248 3D mesa 30 × 30 × 10 μm^3 parallelepiped SVs, fabricated on n-type SOI wafers. The silicon surrounding the SVs was removed using plasma etching technology to avoid any charge sharing between adjacent SVs. Its charge collection properties and response to therapeutic ion beam has been studied thoroughly in Ref. [9,10] The second device is called the "mushroom" microdosimeter and is based on 2,500 full 3D cylindrical SVs with diameter of 30 and 18 μm and height of 9.1 μm, fabricated on p-type SOI wafer utilizing the 3D detector technology.[11] Similar to the bridge microdosimeter, the silicon surrounding the cylindrical volumes has been etched away using the deep reactive ion etching (DRIE) technique. Figure 1(a) shows the bridge microdosimeter mounted on a dual in line (DIL) package and a scanning electron microscope (SEM) image of a section of the microdosimeter, revealing the straight parallelepiped shape SVs. A diagram of a single SV of the mushroom microdosimeter and its SEM image are shown in Figs. 1(b) and 1(c), respectively. The intention of comparing the response of the two microdosimeters in this work was to understand the effect of SV shapes on the microdosimetric spectra and dose-mean lineal energy as well as to introduce the new 3D mushroom microdosimeter for charged particle therapy application. Since the response of the bridge microdosimeter in heavy ion beam has been previously published, the experimental and simulation results of the mushroom microdosimeter will be the focus of this work.

Figure 2 shows the microdosimetric probe, named the Micro Plus probe (μ^+), developed at the CMRP, based on an SOI microdosimeter with an array of 3D SVs connected to a low noise spectroscopy-based readout circuit. The readout electronics of the μ^+ probe is located 10 cm away from the detector to keep the readout circuitry out of the primary radiation field and avoid radiation damage to the electronics. The μ^+ probe is covered by a PMMA sheath to allow the microdosimeter to be operated in water [Fig. 3(a)].

2.B. Passive irradiation at HIMAC facility with ^{14}N and ^{16}O ion pristine BP and ^{12}C ion SOBP

The 180 MeV/u ^{14}N and 400 MeV/u ^{16}O pristine BP beams were delivered at the biological beam line at the heavy ion medical accelerator in Chiba (HIMAC), Japan. A Ta scatterer was used upstream to broaden the beam and for the ^{16}O beam an 86 mm thick PMMA range shifter was placed ~60 cm upstream of the water phantom with the water-equivalent thickness (~100 mm) of the PMMA added to the depth in the phantom. The physical dose of the 180 MeV/u ^{14}N and 400 MeV/u ^{16}O in water was measured using a PTW 31066 (PTW, Freiburg im Breisgau, Germany) pinpoint ionization chamber at the same effective depth of the microdosimeters. The beam was collimated to a 10 × 10 cm^2 field using a brass collimator which is located 16 cm upstream from the water phantom.

A 290 MeV/u ^{12}C ion was delivered with an extended SOBP of 60 mm using an Al ridge filter. A 0.649 mm Ta scatterer was used upstream to broaden the beam and was collimated to 10 × 10 cm^2 with a range of 147.9 mm in water. The microdosimetric probe was mounted in a water phantom using an X–Y stage to remotely control the detector location in the phantom with sub-hundred micron precision [Fig. 3(a)].

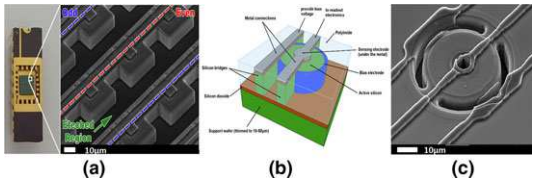

FIG. 1. (a) The CMRP microdosimeter chip in DIL package (left) and SEM image of the bridge microdosimeter sensitive volumes (right). (b) Schematic of a single cylindrical SV of the mushroom microdosimeter, (c) SEM image of the single volume of the mushroom microdosimeter. [Color figure can be viewed at wileyonlinelibrary.com]

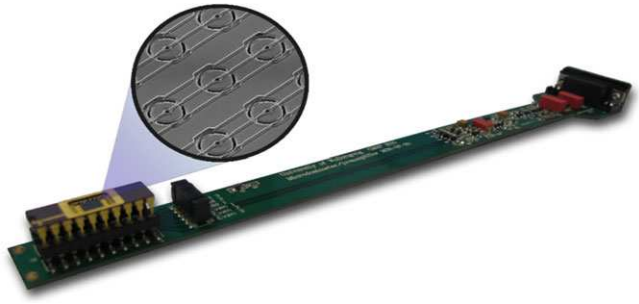

FIG. 2. The microdosimetric probe (or also called MicroPlus probe — μ^+) connected to the microdosimeter chip. [Color figure can be viewed at wileyonlinelibrary.com]

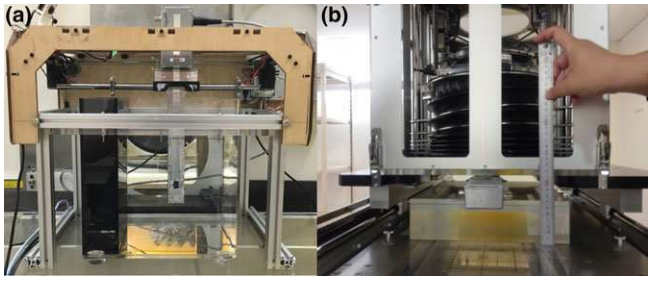

FIG. 3. Experimental setup of the μ^+ probe in HIMAC and Gunma experiment, (a) μ^+ probe mounted on a XY-movement stage in a water phantom. (b) μ^+ probe placed underneath the water column at Gunma. [Color figure can be viewed at wileyonlinelibrary.com]

2.C. Pencil beam scanning irradiation at GHMC with 290 MeV/u ^{12}C ion pristine BP

The mushroom microdosimeter was irradiated at Gunma university heavy ion medical centre (GHMC) facility using a 290 MeV/u ^{12}C pencil beam with an aluminum ripple filter used to broaden the ion's range along the direction of travel. The sigma of the spot beam was 3.3 mm with a beam intensity of approximately 10^6 particles/spill. In this experiment, the μ^+ probe was inserted into a PMMA block to minimize the air gap surrounding the microdosimeter and was placed underneath the water column [Figs. 3(b)], with the beam vertically incident on the microdosimeter. The water level could be adjusted with 0.1 mm increments.

2.D. Data collection and analysis

The spectral response of the detector was recorded with an Amptek MCA 8000A multi channel analyzer (MCA). The energy calibration of the measurement system was performed with an Ortec 419 precision pulse generator which was calibrated with a 300 μm thick planar silicon PIN diode with 100% charge collection efficiency (CCE) in response to 5.486 MeV alpha particles from a ^{241}Am source. To obtain the microdosimetric quantities from this spectrum, the energy deposited was converted to lineal energy which is used to describe the energy deposition in a micron size sensitive volume (SV) along a particles track, given by:

$$y = \frac{\epsilon}{<l>} \tag{1}$$

where ε is the energy deposited in a SV with an average chord length $<l>$. In this work, we adopt the method proposed in Ref. [12] which is to use the mean path length $<l_{Path}>$ instead of $<l>$. The strong directionality of a heavy ion beam makes the use of $<l>$ inappropriate when using SOI designs. The $<l_{Path}>$ considers the mean path of the charged particles when traversing the SV and is determined using Monte Carlo simulations. It was found in Ref. [12] that using the thickness of the SV for in-field depths gave a good approximation to the calculated $<l_{Path}>$ values. Therefore, this approximation was adopted with $<l_{Path}>$ values of 10 and 9.1 μm used for the bridge and mushroom microdosimeter, respectively. Since we are interested in microdosimetric quantities relevant to human tissue, a conversion was therefore necessary to obtain the simulated deposited energy in tissue. A silicon-tissue scaling factor of 0.58 was obtained by calculating the energy deposition in silicon SV exposed to the 290 MeV/u ^{12}C ion radiation field along the Bragg peak curve, by means of Geant4.[12]

The spectrum of stochastic events *f(y)* for all primary and secondary particles generated during an exposure to tissue by ionizing radiation can be derived from the spectrum of energy deposition events. The dose lineal energy distribution *d(y)* is given by:

$$d(y) = \frac{yf(y)}{\overline{y_F}} \tag{2}$$

where $\overline{y_F} = \int_0^\infty yf(y)dy$ and $\overline{y_D} = \int_0^\infty yd(y)dy$; $\overline{y_F}$ is the frequency-mean lineal energy and $\overline{y_D}$ is the dose-mean lineal energy. The latter is used to determine the α parameter in the linear quadratic model (LQM) applied for radiation field of interest and used later as an input parameter for the MKM to calculate RBE_{10} corresponding to 10% human salivary gland (HSG) cell survival. A detailed description for calculating RBE_{10} using the MK model can be found in Ref. [5].

2.E. Geant4 simulations

The Monte Carlo simulation toolkit Geant4 version 10.2p02[13–15] was used to model the mushroom SOI microdosimeters within the HIMAC Bio beamline.[16] For electromagnetic interactions, the G4 Standard EM option 3 Physics List was used and for inelastic hadronic interactions, the binary intranuclear cascade (BIC) model was adopted for both light ions such as protons as well as for heavier ions. The HIMAC Bio beamline (shown in Fig. 4) was modeled with the primary ^{14}N and ^{16}O being generated at the beam duct end which was then shaped to form a uniform circular beam by passing through wobbler magnets, a Ta scatterer, and then collimated to a 10 × 10 cm^2 size when reaching the water phantom. The initial energy of the ^{14}N and ^{16}O ions was 180 and 400 MeV/u with an energy sigma of 0.35% and 0.15%, respectively. The number of primary particles varied slightly depending on where in the phantom the detector was placed, for the oxygen beam there was approximately 10^7 and 10^8 before and after the BP, respectively, while for nitrogen these values were approximately an order of magnitude higher. In the Geant4 simulation, an *Event* corresponds to the generation of a primary particle. At the end of each event the energy depositions (stored in *Geant4 Hits*) of the primary particle

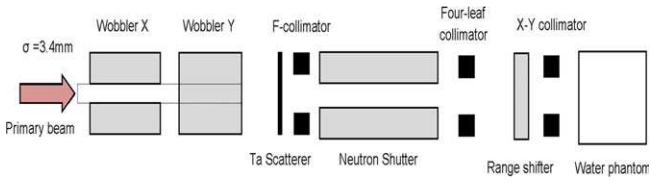

FIG. 4. Diagram of the HIMAC BIO beamline modeled for the simulation (not to scale). [Color figure can be viewed at wileyonlinelibrary.com]

and all of its secondaries in the SVs of the microdosimeter device are summed as individual $Edep_{event}$ for each SV. Each $Edep_{event}$ hit is stored as a separate entry, which, at the end of the simulation, is processed into a histogram of the energy deposition spectrum.

When analyzing the contribution of the secondary radiation field to the microdosimetric spectra, the energy deposition $Edep_{SP}$ of any striking particle (SP) in a SV is counted separately. The SP can be either a primary particle or a secondary track originating outside the SVs. The energy deposition of the secondary particles originated by the SP in the SV is summed to the $Edep_{SP}$. The energy depositions deriving from the same SP traversing multiple SVs is summed and stored as an entry.

3. RESULTS AND DISCUSSION

3.A. Response of the bridge and mushroom microdosimeter in different ion therapy fields

3.A.1. ^{14}N ion pristine BP

Figure 5(a) shows a comparison of the dose-mean lineal energy distributions in water obtained with the bridge and mushroom microdosimeters for the passively delivered 180 MeV/u ^{14}N beam. Both detectors provided consistent $\overline{y_D}$ values of approximately 29.3 keV/μm at 19.5 mm depth in water to approximately 150 keV/μm at the BP (49.5 mm), and then sharply rose up to 438 and 412 keV/μm at the distal part of the BP for the bridge and mushroom microdosimeter, respectively. The variation $\overline{y_D}$ in values obtained with the two detectors at the distal part of the BP was due to a dramatic change in LET of particles toward the BP and in the distal part of the BP. Due to the extremely high spatial resolution of the SOI microdosimeter it was possible to clearly see these transitions in $\overline{y_D}$ values.

Figure 5(b) shows the derived RBE_{10} distribution obtained with the two detectors in water as well as the physical dose measured at the same position using a pin point ionization chamber. It can be seen that at 49.5 mm, the RBE_{10} reached the maximum value of 3.1 and occurred shortly before the maximum physical dose. Detailed RBE_{10} values at the BP can be seen in Fig. 5(c). The RBE_{10} of the beam was calculated to be 1.5 when $\overline{y_D}$ was 29.3 keV/μm. Additionally, the RBE_{10} was 3.1 when $\overline{y_D}$ was approximately 150 keV/μm and at the maximum $\overline{y_D}$ of 438 keV/μm, RBE_{10} was approximately 2.0. The decrease in RBE_{10} toward distal part of the BP is associated with the overkilling effect of cells which has been taken into account by the MK model.[5]

Figure 6 shows the microdosimetric spectra obtained with the μ^+ probe (mushroom microdosimeter) along the central axis of the ^{14}N ion pristine BP. Measurements were taken at depths of 49, 49.5, 50, 50.5, 50.75, 55, 75, 105 mm in water. The microdosimetric spectrum dispersed and shifted to higher lineal energy deposition at the distal edge of the BP

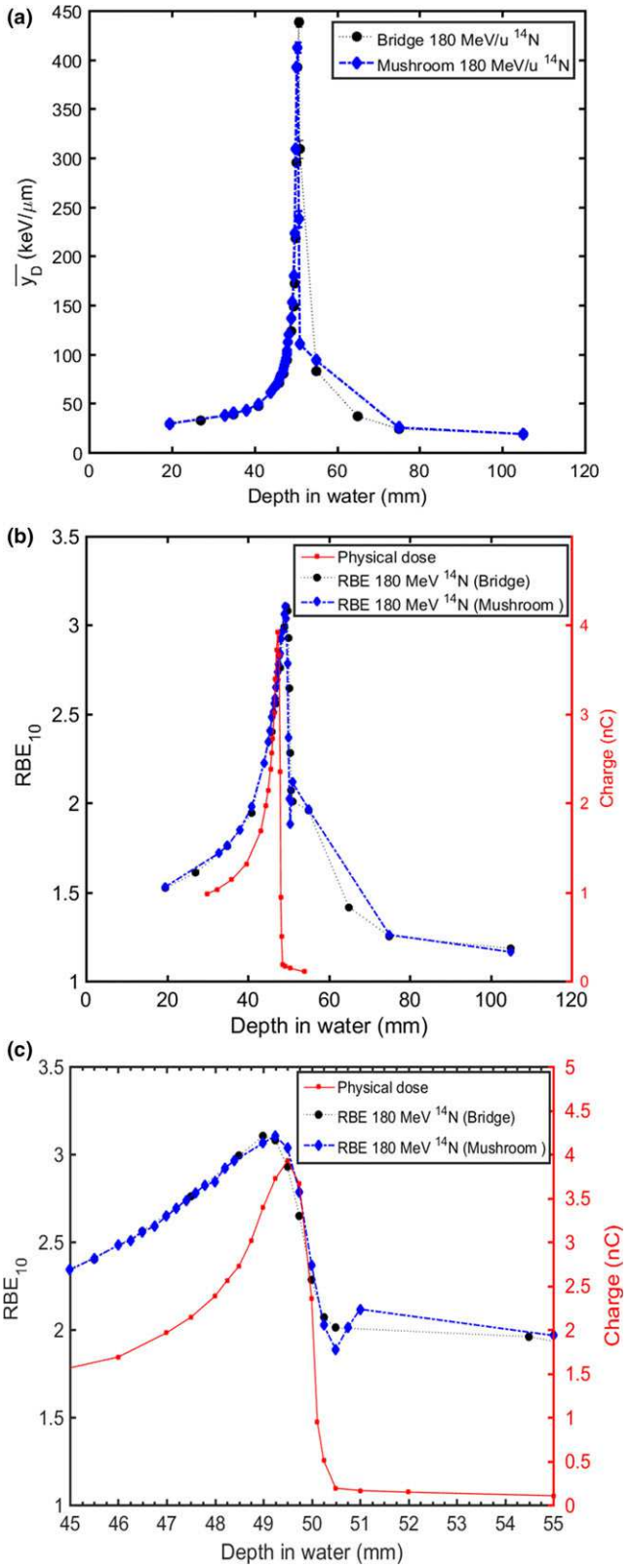

FIG. 5. (a) Dose-mean lineal energy $\overline{y_D}$, (b) RBE_{10} distribution obtained with the bridge and mushroom microdosimeters (μ^+ probe) as a function of depth in water for the 180 MeV/u ^{14}N pristine BP and (c) detailed view of RBE_{10} distribution. [Color figure can be viewed at wileyonlinelibrary.com]

due to the increased LET of primary ions, in addition to the contribution from lighter fragments. A lineal energy variation from approximately 100 to 800 keV/μm was observed at the distal edge of the BP. At 75 and 105 mm depth in water, the spectra were dominated by alpha fragments and recoil protons generated from neutron interactions in water and a small contribution from high LET particles.

Figures 7(a) and 7(b) show a comparison of the microdosimetric spectra obtained with the μ^+ probe (mushroom microdosimeter) and the Geant4 simulation at 46 and 55 mm depth in water, respectively. It can be seen that the simulated microdosimetric spectrum matched reasonably well. The simulated dose weighted microdosimetric spectra of different radiation components in the field are presented in Fig. 7(b) for 55 mm depth in water. A main contribution to the microdosimetric spectrum was from carbon particles, then helium, protons, boron, beryllium and lithium.

3.A.2. ^{16}O ion pristine BP

Figure 8(a) shows a comparison of the experimental and simulated $\overline{y_D}$ distributions in water obtained with the mushroom microdosimeter for the passively delivered 400 MeV/u ^{16}O beam. The $\overline{y_D}$ values were approximately 24 keV/μm at the entrance depth, increasing to 205 keV/μm at the BP and sharply increased to 381 keV/μm at the distal part of the BP. It can be seen that the $\overline{y_D}$ values simulated using Geant4 agreed well with the experimental results at the entrance and toward the BP and distal part of the BP. However, in the downstream region, the simulated $\overline{y_D}$ is lower than the

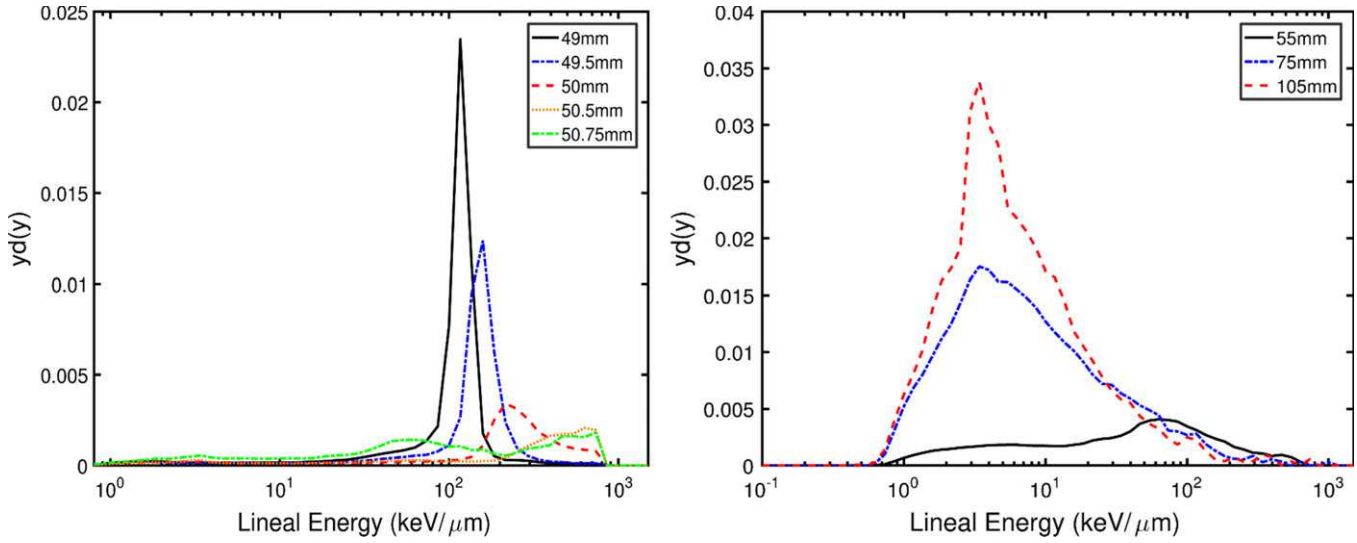

FIG. 6. Microdosimetric spectra obtained with the μ^+ probe (mushroom microdosimeter) at different depths in a water phantom for passively delivered 180 MeV/u ^{14}N ion pristine BP. [Color figure can be viewed at wileyonlinelibrary.com]

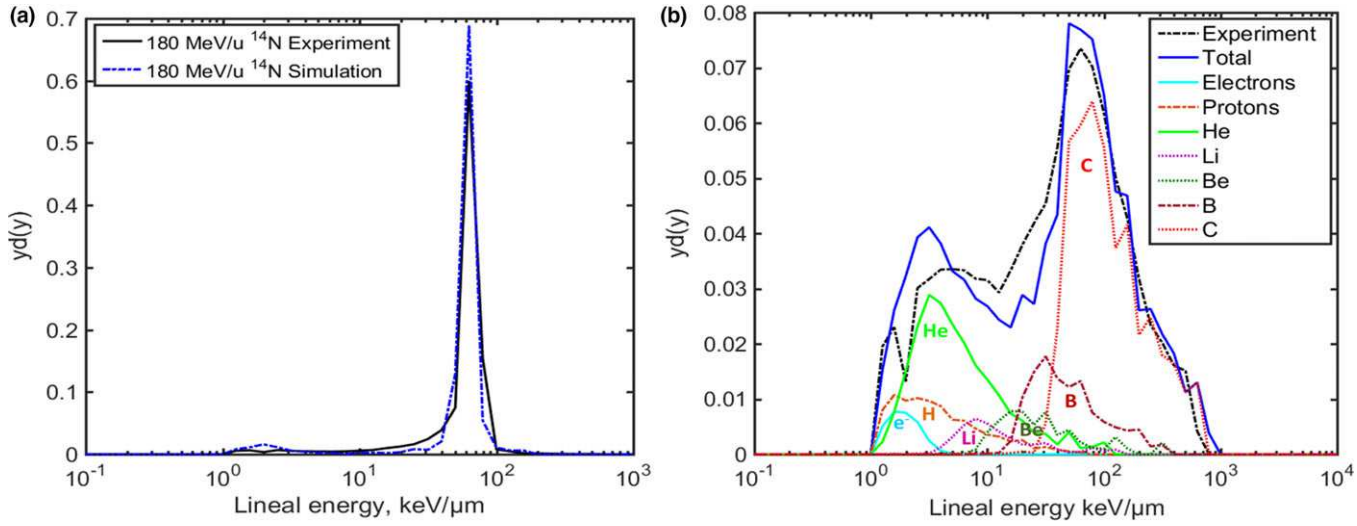

FIG. 7. Microdosimetric spectra obtained with the μ^+ probe mushroom microdosimeter and Geant4 simulation at (a) 46 mm and (b) 55 mm depth in water for 180 MeV/u ^{14}N beam. [Color figure can be viewed at wileyonlinelibrary.com]

experimental values. The lower values observed in the simulation for downstream positions can be attributed to the broader angular distributions of fragments that the BIC model produces for larger fragments compared to the experiment.[17] This is due to lower statistics in the downstream region with rare high-energy deposition events which infrequently occurred but have a strong impact on the spectrum. Figure 8(b) shows the comparison of the Geant4 simulated and microdosimetric measurement-based RBE_{10} for the 400 MeV/u ^{16}O beam. Unlike the $\overline{y_D}$ distribution where the max $\overline{y_D}$ value was observed approximately 1 to 1.5 mm after the BP physical dose, the maximum RBE_{10} of 2.94 occurred just before the BP. This demonstrates that the depth of the maximum RBE_{10} for Nitrogen and Oxygen ions occurs slightly earlier than the maximum physical dose. A detailed view of RBE_{10} values and physical dose distribution at the BP can be seen in Fig. 8(c).

Figure 9 shows the microdosimetric spectra obtained with the μ^+ probe (mushroom microdosimeter) along the central axis of the 400 MeV/u ^{16}O pristine beam. Due to the high spatial resolution of the SOI microdosimeter, measurements with small increments at the BP and distal part of the BP were possible. It can be observed that even with 0.5 to 1 mm increments, the microdosimetric spectra changed dramatically and shifted to higher LET regions. At 191.5 and 192 mm, the dose mean lineal energy deposition from oxygen events ranged mostly from 10 keV/µm to 1000 keV/µm. At the distal part of the BP (193 to 194 mm depth), almost all oxygen ions have stopped, with fragments dominating the microdosimetric spectrum. Further downstream of the BP, the microdosimetric spectrum is gradualy dominated by carbon and alpha fragments as well as fragmented protons and recoil protons produced by neutrons (Fig. 9b).

Figure 10a and 10b show a comparison of the microdosimetric spectra obtained with the μ^+ probe and Geant4 simulation at 170 mm and 195 mm depth in water using a 400 MeV/u ^{16}O ion beam, respectively. Similar to the results with Nitrogen, the experimental microdosimetric spectrum matched with the Geant4 simulation results. Fig 10b shows different components contributing to the microdosimetric spectrum for 195 mm depth. It shows that the main contribution to the spectrum was due to nitrogen, carbon and boron nuclei. The contribution from protons and alpha particles dominated the lower lineal energy region. Negligible contribution from Be and Li ions was observed.

3.A.3. ^{12}C ion pristine and spread out BP

A comparison of the MKM-based RBE_{10} values obtained with the bridge microdosimeter, mushroom microdosimeter, and a TEPC[5] in a 290 MeV/u ^{12}C SOBP of 60 mm is shown in Fig. 11. The RBE_{10} value obtained with the bridge microdosimeter was 1.15 at the entrance and increase to 1.56 at the beginning of the SOBP, then rapidly increased to 2.57 at the distal part of the SOBP. The maximum RBE_{10} obtained by the

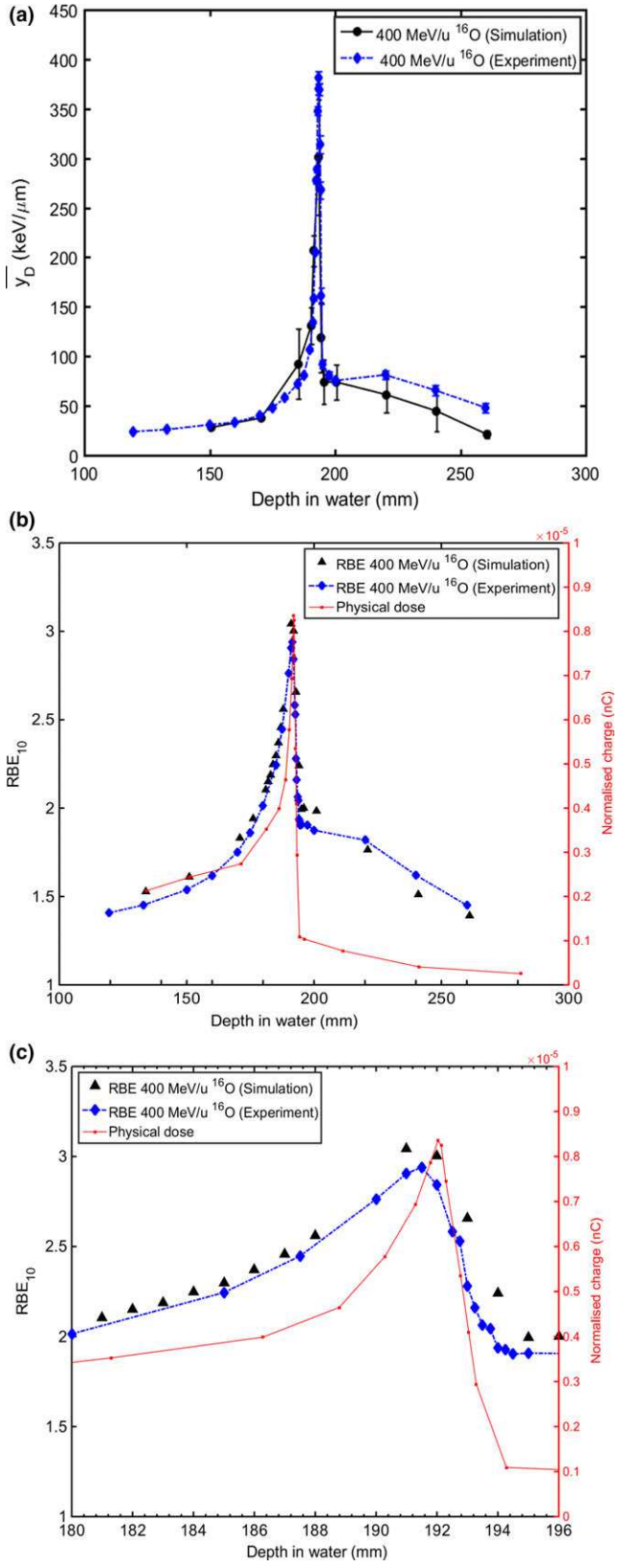

FIG. 8. (a) Experimental and simulation results of dose-mean lineal energy $\overline{y_D}$ and (b) RBE_{10} distribution obtained with the mushroom microdosimeters (μ^+ probe) as a function of depth in water for the 400 MeV/u ^{16}O pristine BP, (c) detailed view of RBE_{10} distribution. [Color figure can be viewed at wileyonlinelibrary.com]

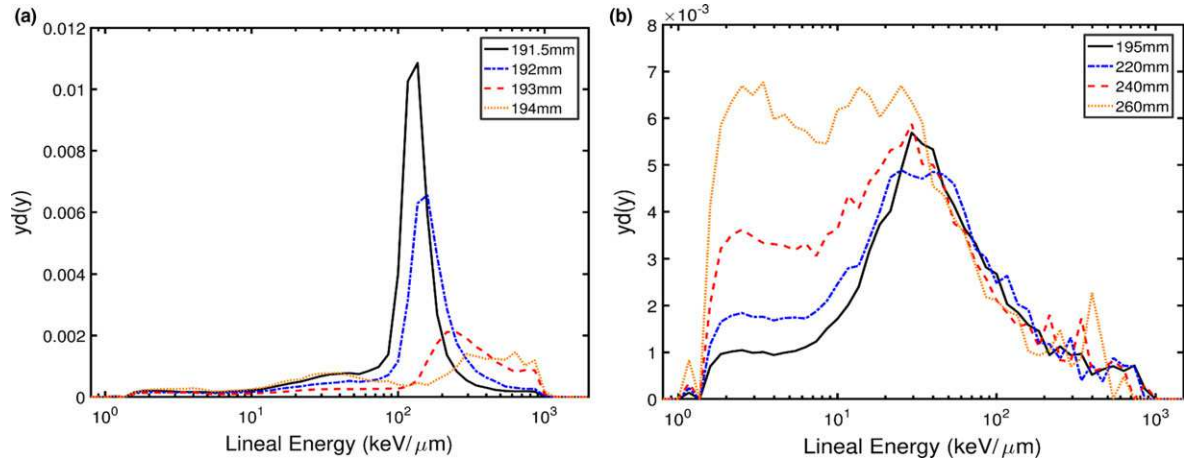

FIG. 9. Microdosimetric spectra obtained with the μ^+ probe (mushroom microdosimeter) at different depths (a) 191.5–194 mm and (b) 195–260 mm in a water phantom for passively delivered 400 MeV/u ^{16}O ion BP. [Color figure can be viewed at wileyonlinelibrary.com]

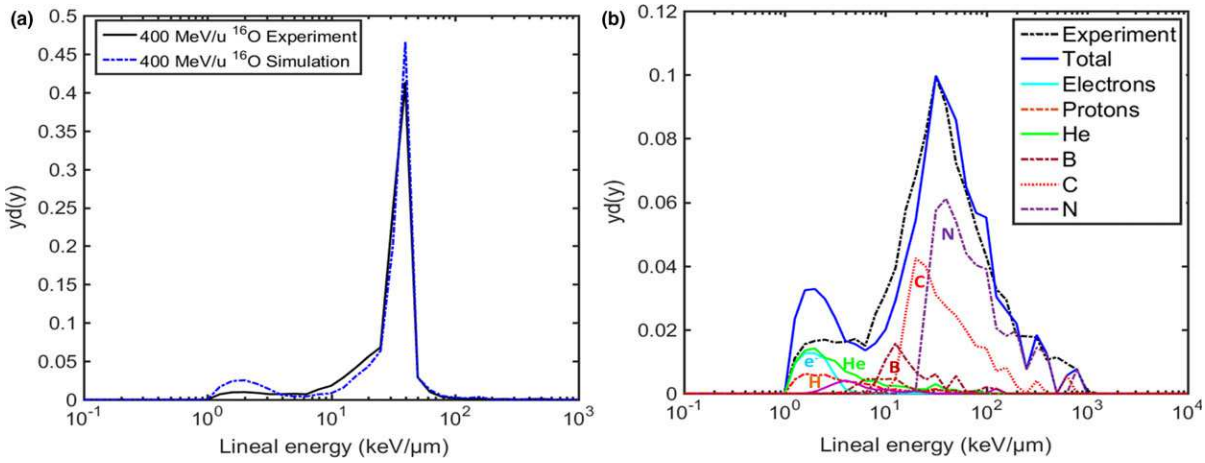

FIG. 10. Microdosimetric spectra obtained with the μ^+ probe mushroom microdosimeter and Geant4 simulation at (a) 170 mm and (b) 195 mm depth in water for 400 MeV/u ^{16}O beam. [Color figure can be viewed at wileyonlinelibrary.com]

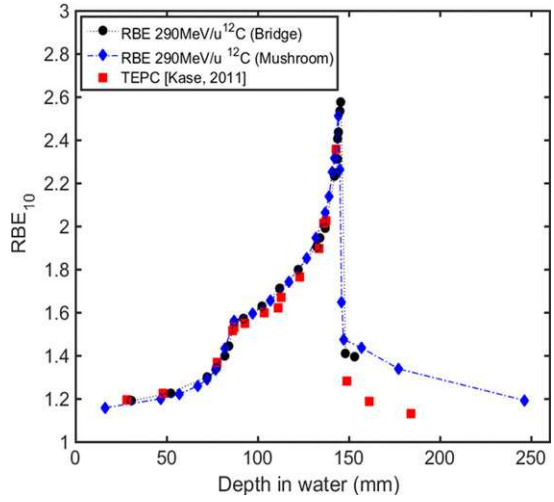

FIG. 11. RBE_{10} distributions obtained with the bridge, mushroom microdosimeters and TEPC in 290 MeV/u ^{12}C SOBP. [Color figure can be viewed at wileyonlinelibrary.com]

TEPC was only 2.3 due to its inability to measure with high spatial resolution at the distal edge of the SOBP. It confirms once again the advantage of using the SOI microdosimeter for high spatial resolution measurements at the distal edge of the SOBP. It has been observed that the RBE_{10} values obtained with the two SOI microdosimeters match quite well with the TEPC measurements, however, much lower RBE_{10} values were measured by the TEPC in the fragmentation tail region downstream of the SOBP. The RBE_{10} values obtained with the TEPC downstream of the SOBP are lower than that the values calculated by the treatment planning system.[5] This discrepancy could be explained by the wall effect of the TEPC used in the study. In fact, the TEPC has A150 plastic wall of 1.27 mm thick and an Al shell of 0.178 mm thick that could stop the lower energy fragments in the wall as well as eliminate new fragments being produced in the wall and produce different secondaries due to difference in composition of A150 plastic and water. The uncertainty in both SOI and TEPC measurements as a result of low event rates in the downstream of the

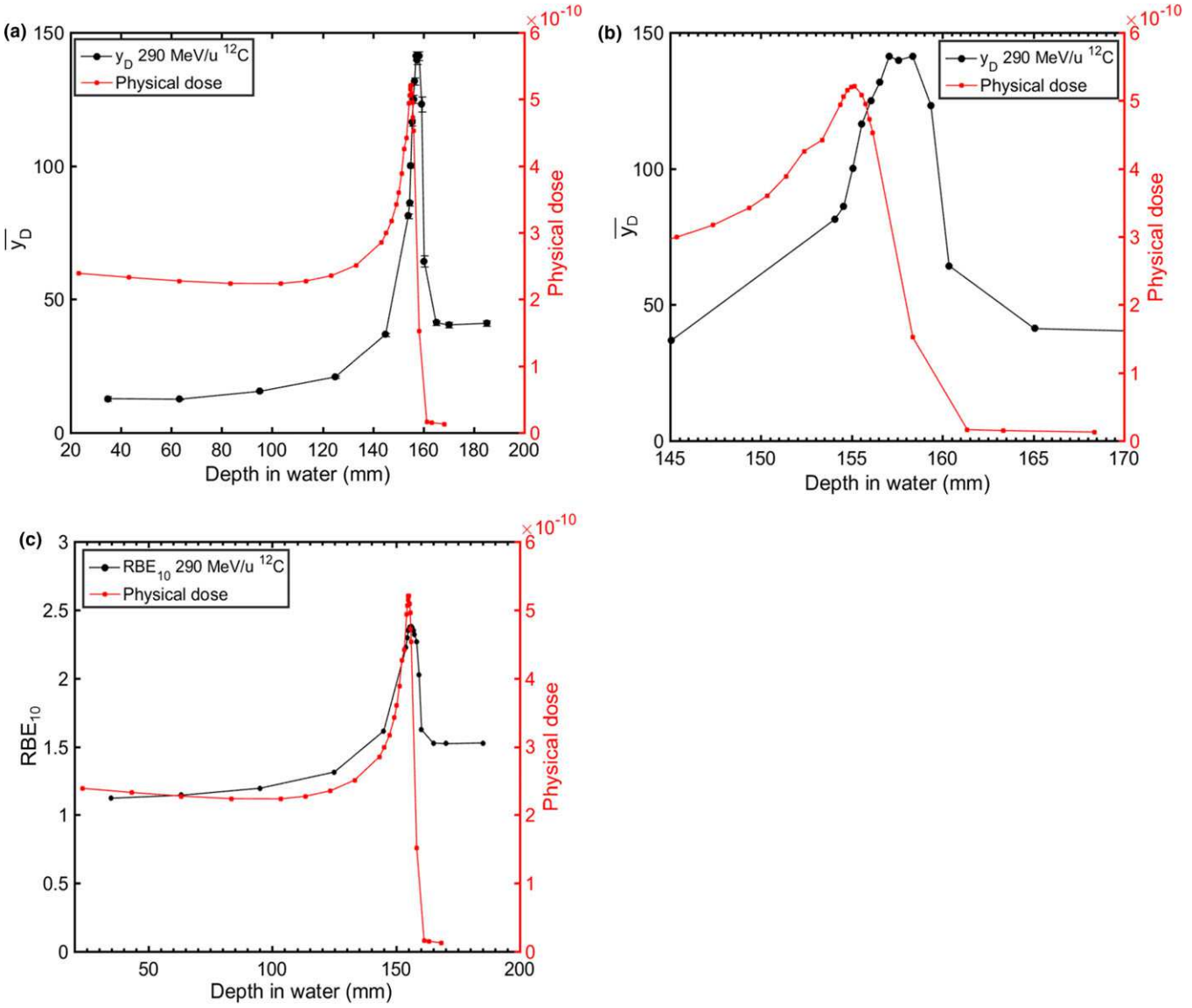

FIG. 12. (a) $\overline{y_D}$ distribution obtained with the mushroom microdosimeter in pencil beam scanning 290 MeV/u ^{12}C (b) detailed view of $\overline{y_D}$ distribution (c) RBE_{10} distribution. [Color figure can be viewed at wileyonlinelibrary.com]

SOBP may also contribute to this discrepancy. It should be noted that in Ref. [5] Geant 4-simulated RBE_{10} values downstream of the SOBP using a TEPC also showed higher RBE_{10} values than measured with TEPC.

Figure 12(a) shows the $\overline{y_D}$ distribution with depth for the 290 MeV/u ^{12}C ion pencil beam at Gunma university heavy ion medical centre (GHMC). The $\overline{y_D}$ value was 13 keV/μm at 35 mm depth in water and then increased with depth up to a maximum $\overline{y_D}$ of 141 keV/μm at 158 mm depth, then sharply decreased when carbon ions fully stopped in the water phantom before reaching the detector. It can be seen that the maximum $\overline{y_D}$ occurred slightly behind the maximum physical dose. The physical dose along the BP was measured by a Markus ionization chamber along the central axis of the pencil beam scanning. Figure 12(b) shows a detailed view of the $\overline{y_D}$ distribution at the BP, measured with submillimeter spatial resolution. It can be seen that the $\overline{y_D}$ distribution at the peak illustrates the effect of the ripple filter used in this facility which is impossible to observe with any TEPC based microdosimeters. Figure 12(c) shows the RBE_{10} distribution of the scanning carbon ion beam. It was observed that unlike nitrogen and oxygen ions presented above, the maximum RBE_{10} value of the carbon ions occurred at the same depth with the maximum physical dose, which is an advantage of using carbon ion for cancer patient treatment. This has been emphasized by Kraft,[2] however, it was impossible to confirm earlier with experimental measurements using the TEPC.

4. CONCLUSION

New SOI microdosimeters have been characterized in charged particle beams with ^{12}C, ^{14}N, and ^{16}O ions. The dose-mean lineal energy and RBE_{10} distributions in water

were obtained with exceptionally high spatial resolution at the BP and distal part of the BP. This work has shown that the $\overline{y_D}$ at the entrance of the Nitrogen and Oxygen BP was about 24–29 keV/μm and the maximum $\overline{y_D}$ values went up to approximately 400 keV/μm. The maximum RBE_{10} values for ^{14}N and ^{16}O ions occurred just before the maximum physical dose BP. Carbon ions have been shown to have a smaller entrance dose-mean lineal energy of 14 keV/μm and RBE_{10} occurring at the same position as the maximum physical dose (BP). These findings are important for accurate biological dose prediction using different therapeutic ion beams.

Geant4 simulation results of microdosimetric spectra, $\overline{y_D}$ and RBE_{10} distributions were in very good agreement with the experimental results for in-field positions. Larger uncertainty in the downstream region of the BP was observed due to lower event rates which cause slight discrepancies between the simulation and experimental results.

The results obtained by the two types of SOI microdosimeters were very similar, no essential difference in the derived RBE_{10} was observed between the bridge and mushroom microdosimeters while the shape of their 3D SV is different (rectangular parallelepiped and cylinder, respectively) but their thicknesses are the same. It has been demonstrated that the mushroom microdosimeter is suitable to use in heavy ion therapy applications.

This study presented a new and fast radiation field characterization tool in heavy ion therapy for pencil beam scanning and passive delivery systems using a silicon microdosimeter containing 3D SVs. No pile up was observed in the ^{12}C ion pencil beam scanning measurements where dose rate is two orders of magnitude higher than in a passive beam delivery. This microdosimetric probe has been applied to proton and ion beam characterization with submillimeter spatial resolution and shows promise as an experimental device used for microdosimetric spectra measurements and based on this, commissioning of RBE used in treatment planning system.

ACKNOWLEDGMENTS

This research was supported by the Australian Government through the Australian Research Council's Discovery Projects funding scheme (project DP 170102273). The authors acknowledge Dr. Nadia Court and her team at the UNSW ANFF node for their packaging work as well as Mr. Adam Sarbutt from the Institute of Materials Engineering, ANSTO and Mr. Peter Ihnat from the School of Physics, UOW for their assistance in preparation for the experiment. We thank the University of Wollongong Information Technology Services (ITS) for computing time on the UOW High Performance Computing Cluster and the Australian National Computational Infrastructure (NCI) for computing time on the Raijin cluster. Finally the authors also thank all collaborators in 3D-MiMiC project, funded by the Norwegian Research Council via the NANO2021 program.

CONFLICT OF INTEREST

The authors have no conflicts to disclose.

[a)]Authors to whom correspondence should be addressed. Electronic mails: tltran@uow.edu.au; anatoly@uow.edu.au.

REFERENCES

1. Tommasino F, Scifoni E, Durante M, Sisterson M. New ions for therapy. *Int J Part Ther*. 2015;2:428–438.
2. Kraft G. Tumor therapy with heavy charged particles. *Progr Part Nucl Phys*. 2000;45:473–544.
3. Bortot D, Pola A, Agosteo S, et al. A miniaturized alpha spectrometer for the calibration of an avalanche-confinement TEPC. *Radiat Measur*. 2017;106:531–537.
4. Martino G, Durante M, Schardt D. Microdosimetry measurements characterizing the radiation fields of 300 MeV/u ^{12}C and 185 MeV/u ^{7}Li pencil beams stopping in water. *Phys Med Biol*. 2010;55:3441–3449.
5. Kase Y, Kanai T, Matsumoto Y, et al. Microdosimetric measurements and estimation of human cell survival for heavy-ion beams. *Radiat Res*. 2006;166:629–38.
6. Agosteo S, Fallica P, Fazzi A, et al. A pixelated silicon telescope for solid state microdosimetry. *Radiat Meas*. 2008;43:585–589.
7. Wroe A, Schulte R, Fazzi A, Pola A, Agosteo S, Rosenfeld A. Direct RBE estimation of radiation fields using a ΔE-E telescope. *Med Phys*. 2009;36:4486–4494.
8. Rosenfeld A. Novel detectors for silicon based microdosimetry, their concepts and applications. *Nucl Instrum Meth Phys Res A*. 2016;809:156–170.
9. Tran L, Chartier L, Prokopovich D, et al. 3D-mesa "bridge" silicon microdosimeter: charge collection study and application to RBE studies in ^{12}C radiation therapy. *IEEE Trans Nucl Sci*. 2015;62:504–511.
10. Tran L, Chartier L, Bolst D, et al. 3D silicon microdosimetry and RBE study using ^{12}C ion of different energies. *IEEE Trans Nucl Sci*. 2015;62:3027–3033.
11. Parker I, Kenney CJ, Segal J. 3D – a proposed new architecture for solid-state radiation detectors. *Nucl Instrum Meth Phys Res A*. 1997; A395:328–343.
12. Bolst D, Guatelli S, Tran LT, et al. Correction factors to convert microdosimetry measurements in silicon to tissue in ^{12}C ion therapy. *Phys Med Biol*. 2017;62:2055–2069.
13. Allison J, Amako K, Apostolakis J, et al. Geant4 developments and applications. *IEEE Trans Nucl Sci*. 2006;53:270–278.
14. Agostinelli S, Allison J, Amako K, et al. Geant4 – a simulation toolkit. *Nucl Instrum Meth Phys Res, Sect A*. 2003;506:250–303.
15. Allison J, Amako K, Apostolakis J, et al. Recent developments in Geant4. *Nucl Instrum Meth Phys Res, Sect A*. 2016;835:186–225.
16. Torikoshi M, Minohara S, Kanematsu N, et al. Irradiation system for HIMAC. *Radiat Res*. 2007;48:15–25.
17. Bolst D, Cirrone G, Cuttone G, et al. Validation of Geant4 fragmentation for heavy ion therapy. *Nucl Instrum Meth Phys Res A*. 2017;869:68–75.